PERGAMON

International Journal of Heat and Mass Transfer 42 (1999) 415–422

International Journal of HEAT and MASS TRANSFER

Numerical investigations of the compressible flow and the energy separation in the Ranque–Hilsch vortex tube[1]

W. Fröhlingsdorf, H. Unger*

Lehrstuhl für Nukleare und Neue Energiesysteme (NES) der Ruhr-Universität-Bochum (RUB), Germany

Received 15 October 1997; in final form 26 May 1998

Abstract

In the Ranque–Hilsch vortex tube a compressible fluid (e.g., air) experiences an expansion process leading to separation into a cold and hot gas stream. The compressible flow and energy separation phenomena are simulated numerically by using the code system CFX. In order to calculate successfully the energy separation, the numerical model had to be extended by integrating relevant terms for the shear-stress-induced mechanical work. An axisymmetric model was developed, allowing a successful post-calculation of experimental results.

Nomenclature

A area [m^2]
c_p specific heat at constant pressure [J kg^{-1} K^{-1}]
E_V change of energy per unit volume with respect to time [W m^{-3}]
h enthalphy [J kg^{-1}]
H total specific enthalpy [J kg^{-1}]
k turbulence kinetic energy [m^2 s^{-2}]
l length [m]
Ma_i inlet Mach number
$\dot{M}$ mass flow rate [kg s^{-1}]
p pressure [bar]
Pr_T turbulent Prandtl number
r, θ, z cylindrical coordinates [m]
$Re_{\theta,p}$ tangential Reynolds number
T temperature [K]
t time [s]
v velocity [m s^{-1}]
v_θ tangential velocity [m s^{-1}]
v_r radial velocity [m s^{-1}]
v_z axial velocity [m s^{-1}].

Greek symbols

ε turbulence dissipation rate [m^2 s^{-3}]
λ thermal conductivity [W m^{-1} K^{-1}]
μ dynamic viscosity [kg m^{-1} s^{-1}]
ξ mass flow fraction
ρ density [kg m^{-3}]
σ stress [N m^{-2}]
τ shear stress [N m^{-2}]
ω angular velocity [s^{-1}].

Subscripts

c cold gas
D diffusion
h hot gas
i inlet in the vortex tube
L laminar
M mechanical energy
p compressed inlet air
ref constant reference value
t total
T turbulent
r, θ, z radial, tangential, axial
0 tube radius, tube length
1 first iteration
2 second iteration.

* Corresponding author. Fax: 0234-7094-158; E-mail: sys-adm@nes.ruhr-uni-bochum.de

[1] Dedicated to Professor J. U. Keller, University of Siegen, Germany, on the occasion of his 60th birthday.

0017–9310/98 $19.00
PII: S0017–9310(98)00191–4

1. Introduction

The separation of a gas stream into a cold and a hot fraction by means of a vortex tube reported for the first time by Ranque [1]. His design of the vortex tube has later been improved by the German physicist Hilsch [2], who arranged a diaphragm at the cold gas site. A qualitative set-up of the vortex tube is shown in Fig. 1. The compressed air in the ring chamber (State **p** in Fig. 1) enters the vortex tube tangentially through the inlet nozzles and develops an approximately axisymmetric vortex flow. From State **p** to **i** the compressible fluid expands and accelerates. Under the influence of centrifugal forces the injected gas is pressed towards the tube wall. Close to the wall the helical gas flow (Fig. 1) is directed to the hot gas outlet. From State **i** to **h** the gas is heated by dissipation (friction), especially near the tube wall, where the velocity gradients are highest. Cold gas is formed by radial expansion towards the center line of the vortex tube. As depicted in Fig. 1, the cold gas flows to the cold gas exit (State **c**) along helical stream lines. The temperature of the hot gas leaving the vortex tube is well above those at the gas inlet, while the cold gas is well below it. As an example (Camiré [3]), for air at 3 bar absolute and 290 K at the inlet, a hot gas temperature of $T_h = 330$ K and a cold gas temperature of $T_c = 260$ K has been obtained.

The energy separation augments with an increase of the pressure relation from inlet to cold gas pressure p_p/p_c (inlet—cold gas condition p,c in Fig. 1). According to experimental results obtained by Stephan [4], the difference between the inlet and the cold gas total temperature $\Delta T_{t,c}$ increases from $\Delta T_{t,c} = -27$ K at an inlet pressure of $p_p = 3$ bar to $\Delta T_{t,c} = -38$ K at $p_p = 5$ bar (cold gas fraction in both cases 30% of the total mass flow at the gas inlet). The total specific enthalpy difference $\Delta H_{c,p}$ of the cold gas **c** compared to the compressed inlet gas **p** describes the change of the mass specific thermal and mechanical energy against the inlet condition:

$$\Delta H_{c,p} = c_p \Delta T_{t,c,p} = c_p \Delta T_{c,p} + \frac{v_c^2}{2} \tag{1}$$

The velocity increases from approximately $v_p \approx 0$ m s^{-1} in the ring chamber to the cold gas velocity v_c. As a consequence the kinetic energy rises ($v_c^2/2 > 0$) and the thermal energy decreases ($c_p \Delta T_{c,p} < 0$). For the cold gas the total enthalpy decreases compared to those of the compressed inlet gas **p**, because the thermal energy decrease exceeds the kinetic energy increase due to kinetic energy transfer to the outer region by means of friction forces (shear stresses). Consequently, in the hot gas both the kinetic and thermal energy rise and the total enthalpy exceeds those of the inlet gas.

2. Transport of mechanical energy

Therefore, for the formation of substantial temperature differences in the vortex tube an energy exchange between cold and hot gas is responsible. The temperature decrease due to expansion is comparable to those in a turbine. Although in the vortex tube are no rotating walls, there are rotating fluid layers exchanging mechanical energy by friction. A model of this mechanism is represented in Fig. 2. The radially expanding cold gas increases its angular velocity ω_c, i.e., the inner layers rotate faster than the outer ones. The shear stresses produce an outwards directed mechanical energy flux E_M (definition and transport of mechanical work are described by Rogowski [5] and Heinisch [6]). The hot gas receives this energy, which predominantly dissipates around the boundary layer of the tube wall. The diffusive energy flux E_D however is directed inwards.

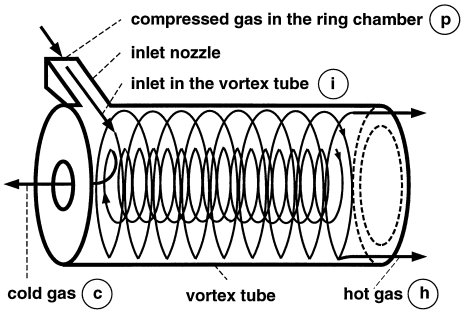

Fig. 1. Qualitative set-up of the Ranque–Hilsch vortex tube. Simplified representation of the helical stream lines for hot and cold gas.

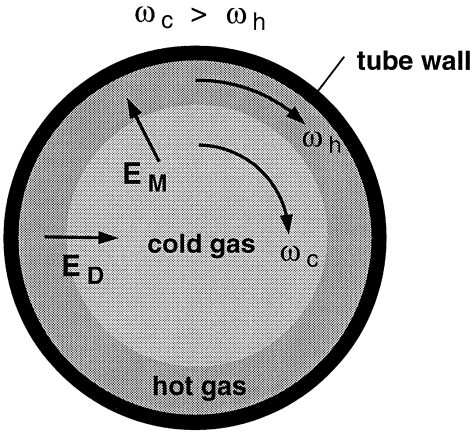

Fig. 2. Schematic representation of the radial energy fluxes in the vortex tube (E_M: mechanical energy flux, E_D: diffusive energy flux).

The rate of work done by viscous forces on a volume element is $-\nabla\cdot[\tau\cdot v]$. The essential shear stress:

$$\tau_{r\theta} = -\mu r\frac{\partial\omega}{\partial r} = -\mu\left(\frac{\partial v_\theta}{\partial r} - \frac{v_\theta}{r}\right), \tag{2}$$

in the vortex flow is directed tangentially and is produced by fluid layers rotating with different angular velocities. If the flow in the vortex tube is assumed to be axisymmetric, the shear stress $\tau_{r\theta}$ causes the differential mechanical work flux:

$$\mathrm{d}E_M = v_\theta\tau_{r\theta}\mathrm{d}A_r = -\mu\left(\omega r^2\,\frac{\partial\omega}{\partial r}\right)\mathrm{d}A_r, \tag{3}$$

which is transferred through the differential surface $\mathrm{d}A_r$ of the cylinder with the radius r and the length $\mathrm{d}z$. In the vortex tube flow (Chapter 3) the angular velocity decreases in radial direction (negative gradient $\partial\omega/\partial r$). The mechanical work flux E_M, directed radially outwards (see Fig. 2), is partially compensated by the diffusive energy flux E_D directed radially inwards.

3. Numerical model and application

The compressible and turbulent vortex tube flow has been investigated numerically by [7] with the code system CFX (finite volume program from AEA Technology). This program allows the calculation of compressible and turbulent flow. The basic set of equations solved by CFX comprises conservation of mass, momentum and energy, expressed as balance equations for the change of mass, momentum and energy per unit volume with respect to time (CFX-Manual [8] and Bird [9]). These are the continuity equation

$$\frac{\partial\rho}{\partial t} + \nabla\cdot(\rho v) = 0, \tag{4}$$

the momentum equation (the gravity is neglected)

$$\frac{\partial\rho v}{\partial t} + \nabla\cdot(\rho v\otimes v) = \nabla\cdot\sigma_T \tag{5}$$

where

$$\sigma = -p\delta + \mu_T(\nabla v + (\nabla v)^T) = -p\delta - \tau_T \tag{6}$$

is the stress tensor, and the energy equation (the gravity is neglected again)

$$\frac{\partial\rho H}{\partial t} + \nabla\cdot[\rho v H] = \frac{\partial p}{\partial t} + \underbrace{\nabla\cdot\left[\left(\frac{\lambda}{c_p} + \frac{\mu_t}{Pr_T}\right)\nabla H\right]}_{E_{V,D}} - \underbrace{\nabla\cdot[\tau_T\cdot v]}_{E_{V,M}}, \tag{7}$$

where

$$H = h + \frac{v^2}{2} + k \tag{8}$$

with the specific static enthalpy h, the specific kinetic energy $v^2/2$ and the specific turbulence kinetic energy k. The terms $E_{V,D}$ and $E_{V,M}$ describe the specific energy change through turbulent diffusion (Index D) and turbulent mechanical work transfer (Index M). As stated above, friction forces cause mechanical energy transfer, which is superimposed and partially compensated by counter current heat transfer mainly due to diffusion processes. The turbulent diffusion can be based on the turbulent Prandtl number $Pr_T = c_p\,\mu_T/\lambda_T$. The relation of the mechanical work flux to the diffusive energy flux (E_M/E_D) increases in the numerical model (see equation (7)) with the turbulent Prandtl number. Therefore, the turbulent Prandtl number is a governing parameter for the strength of the energy separation (Chapter 3).

Fulton [10] states, that the work flux directed outwards is higher than the heat transfer directed inwards. The relation of the radial energy fluxes (E_M/E_D) is influenced by unsteady effects. Experimental results show, that periodical resp. turbulent fluctuations influence the energy transfer in the vortex tube essentially. Measurements from Kurosaka [11] show clearly, that the suppression of the vortex whistle at a turned frequency leads to a decrease of the energy separation. The influence of unsteady effects can indirectly be considered in the numerical model by increasing the turbulent Prandtl number.

The vortex tube flow was investigated by modelling the Bruun-experiment [12] with the CFX code. The essential geometric dimensions and boundary conditions of the experiment were:

- tube length $l_0 = 520$ mm,
- tube radius $r_0 = 47$ mm,
- radius of cold gas outlet orifice $r_c = 17.5$ mm,
- inlet area $A_i = 363$ mm^2 (4 nozzles),
- inlet mass stream $\dot{M}_p = 0.12$ kg/s,
- inlet pressure $p_p = 2$ bar (absolute),
- inlet total temperature $T_{t,p} = 294$ K,
- cold gas fraction $\xi_k = 0.23$,
- cold gas total temperature difference $\Delta T_{t,c,p} = -20$ K,
- hot gas total temperature difference $\Delta T_{t,w,p} = +6$ K.

The numerical axisymmetric calculation model is represented in Fig. 3. The inlet mass flow

$$\dot{M}_p = \dot{M}_i = \rho_i v_{r,i} A_i = 0.12\ \mathrm{kg/s}, \tag{9}$$

is given by the radial velocity $v_{r,i} = 19.4$ m s^{-1}. The mass flow can be defined at the outlet of the inlet nozzle for compressible flow, because the inlet density for air under normal conditions,

$$\rho_{i,ref} = \frac{p_{ref}}{RT_i} = \frac{1.013\cdot10^5}{287\cdot274.3}\frac{\mathrm{kg}}{\mathrm{m}^3} = 1.29\,\frac{\mathrm{kg}}{\mathrm{m}^3}, \tag{10}$$

at the nozzle outlet is set constant by the CFX code. Hence, the reference pressure p_{ref} corresponds to the ambient pressure specified. The inlet Mach number

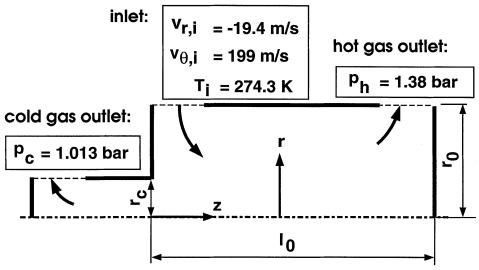

Fig. 3. Axisymmetric CFX-model with boundary conditions at the inlet and outlets for calculation of the vortex tube experiment from Bruun.

$Ma_i = 0.6$ can be calculated with the inlet tangential velocity $v_{\theta,i} = 199$ m s^{-1}, the inlet temperature $T_i = 274.3$ K and the speed of sound $a_i = 332$ m s^{-1}. The inlet total temperature then results to $T_{t,i} = 294$ K. Constant pressure conditions can be assigned to the radially positioned inlet and outlet openings (see Fig. 3). The energy separation is calculated independently by extrapolation of the velocities v_c resp. v_h and the temperatures T_c resp. T_h at the outlets. The temperature and velocity differences related to the inlet allow the calculation of the total temperature differences $\Delta T_{t,i\text{-}c}$ resp. $\Delta T_{t,i\text{-}h}$, by equation (1), between the inlet **i** and the outlets **c**, resp. **h**. The pressure difference of 0.37 bar between the hot and cold gas outlet leads to a cold gas mass flow fraction of $\xi_c = \dot{M}_c/\dot{M}_i = 0.24$. The tube walls are considered to be adiabatic and the no-slip condition is used.

The application of the k–ε-turbulence model leads to substantial differences between measured and calculated tangential velocity profiles (Fig. 4). The dissipation in the inner region is too large (the calculated turbulent viscosity is up to 2000 times higher than the laminar viscosity) for the measured, radially inwards directed transfer of the maximal tangential velocity. At the hot gas end of the vortex tube (dimensionless tube length $z/l_0 = 0.98$) the maximal tangential velocity is located by the dimensionless radius $r/r_0 = 0.925$. The measurements from Bruun show in Fig. 4 that the maximal tangential velocity of $v_0 = 161$ m s^{-1} occurs at the dimensionless radius $r/r_0 = 0.6$.

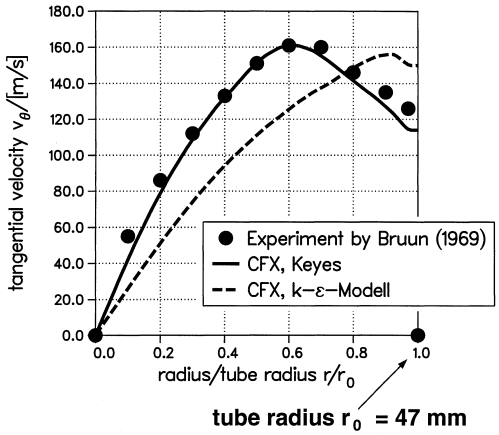

Fig. 4. Comparison code—experiment: tangential velocity profiles calculated by using the k–ε-turbulence model or the correlation from Keyes (see equation (11), dimensionless tube length $z/l_0 = 0.98$, $z = 509.6$ mm).

A much better approximation of the measured results can be achieved, when the k–ε-turbulence model is replaced by the correlation from Keyes [13]:

$$\frac{\mu_T}{\mu_L} = 2.03 \cdot 10^{-3} Re_{\theta,p}^{0.86},$$

$$Re_{\theta,p} = \frac{2 r_p v_{\theta,p} \rho_p}{\mu_L}. \tag{11}$$

The relation from turbulent to laminar viscosity μ_T/μ_L depends on the Reynolds number $Re_{\theta,p}$. The peripheral (Index p) tangential velocity $v_{\theta,p}$ and peripheral density ρ_p were located by Keyes close to the tube wall. In the CFX Model (see Fig. 5) for the calculation of the Reynolds number according to equation (11) the numerical results of the peripheral tangential velocity $v_{\theta,p}$ and peripheral density ρ_p in both finite volumes close to the wall (directly behind the inlet and before the hot gas outlet) were used. The arithmetic mean was used as the constant turbulent viscosity in the whole grid.

For the numerical solution of the equations for the conservation of mass, momentum and energy (see equations (4)–(8)) for compressible flow, an adaptive time stepping procedure with 600 time steps was used (real time of the numerical calculation: 0.36 s, time steps: 0.4–0.8 ms). It is necessary to solve this problem by two iterations, because the specification of pressure values (Dirichlet boundary condition) at both outlets leads to numerical instabilities. In the first iteration procedure at the hot gas outlet the radial velocity was specified by

$$v_{r,h,1} = \frac{\xi_{h,1} \dot{M}_i}{\rho_{h,ref,1} A_h} = \frac{0.77 \cdot 0.12}{1.2 \cdot 4.8 \cdot 10^{-3}} \frac{\text{m}}{\text{s}} = 16 \frac{\text{m}}{\text{s}}, \tag{12}$$

with the constant hot gas density:

$$\rho_{h,ref,1} = \frac{p_{ref}}{R T_{ref}} = \frac{1.013 \cdot 10^5}{287 \cdot 294} \frac{\text{kg}}{\text{m}^3} = 1.2 \frac{\text{kg}}{\text{m}^3}, \tag{13}$$

where the reference values of pressure $p_{ref} = 1.013$ bar and $T_{ref} = 294$ K corresponds with the specified ambient values. The specification of the radial velocity at the hot gas outlet gives information about the hot gas flow fraction to the numerical model and gives the possibility to adjust the cold gas flow fraction:

$$\xi_{c,1} = \frac{\dot{M}_c}{\dot{M}_i} = 1 - \xi_h = 1 - \frac{\rho_{h,ref,1} v_{r,h,1} A_h}{\dot{M}_i} = 0.23. \tag{14}$$

In the second iteration procedure the calculated hot gas pressure $p_{h,1} = 1.38$ bar (see Fig. 3) of the first iteration

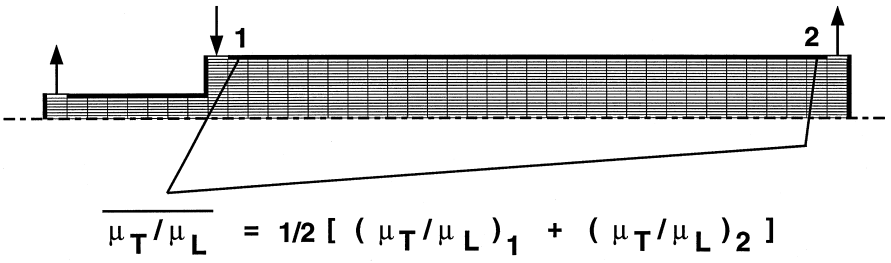

Fig. 5. Grid with representation of the arithmetic mean of the relation μ_T/μ_L after the correlation from Keyes (see equation (11)).

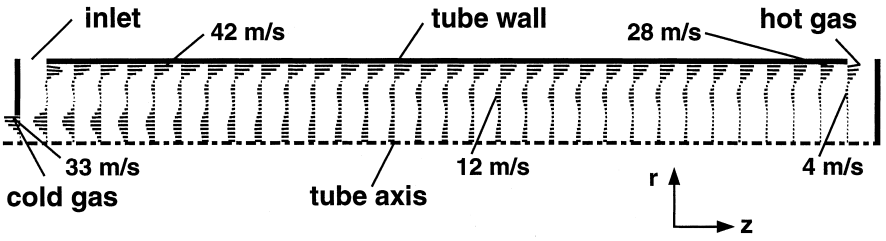

Fig. 6. Velocity profiles of the CFX calculation.

was specified at the hot gas outlet ($p_{h,2} = p_{h,1}$). The numerical results of the first step were given as initial start conditions for the second iteration. The calculated hot gas temperature is $T_{h,2} = 293$ K and the hot gas density:

$$\rho_{h,2} = \frac{p_{h,2}}{RT_{h,2}} = \frac{1.38 \cdot 10^5}{287 \cdot 293}\frac{\text{kg}}{\text{m}^3} = 1.64\frac{\text{kg}}{\text{m}^3}. \quad (15)$$

In the second step, compared to the first step the hot gas density increases (see equations (13) and (15)) and the hot gas radial velocity decreases (see equation (12)) to $v_{r,h,2} = 11.6$ m s^{-1}. The calculated cold gas flow fraction $\xi_{c,2} = 0.24$ corresponds approximately with the experimental cold gas flow fraction $\xi_c = 0.23$.

4. Results

The inlet total pressure:

$$p_{t,i} = p_i + \frac{\rho_i}{2}v_i^2 = p_i\left(1 + \frac{v_i^2}{2RT_i}\right) = 1.88 \text{ bar} \quad (16)$$

calculated from the numerical results of the inlet pressure $p_i = 1.5$ bar and the inlet boundary conditions—velocity $v_i = 200$ m s^{-1} and temperature $T_i = 274.3$ K—is smaller than that measured by Bruun in the air inlet tube ($p_p = 2$ bar), while the pressure loss in the vortex generator, from state **p** to state **i** (see Fig. 1), is not included in the numerical model.

Velocity profiles are shown in Fig. 6, the axial and radial flow patterns are sketched in Fig. 7. The length of the lines in Fig. 6 are proportional to the magnitude of the velocity. The outer stream is directed to the hot gas outlet and the inner stream to the cold gas outlet. Close to the wall the radially expanding fluid causes an axial velocity decrease from 42 m s^{-1} to 28 m s^{-1}. The backflow to the cold gas outlet can be divided into an inner and outer part. In the outer part the axial velocity increases from 4 m s^{-1} at the hot gas outlet to maximal 12 m s^{-1}. In the inner part the axial velocity increases to maximal 33 m s^{-1} at the cold gas outlet.

The mass flow fractions given in Fig. 7 are related to the inlet mass flow. The rotating air enters the vortex tube radially and is pressed towards the tube wall under the influence of centrifugal forces and flows axially directed to the hot gas outlet. In the area of the hot gas outlet the fluid is divided into the hot gas fraction $\xi_w = 0.76$ and the radially inwards expanding part of

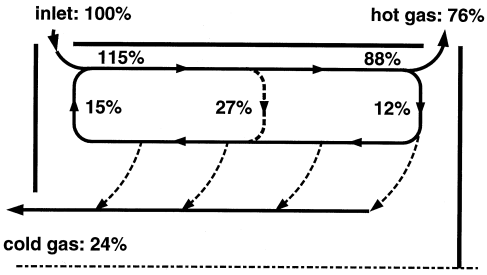

Fig. 7. Axial and radial flow patterns of the vortex tube flow, calculated from the numerical CFX results.

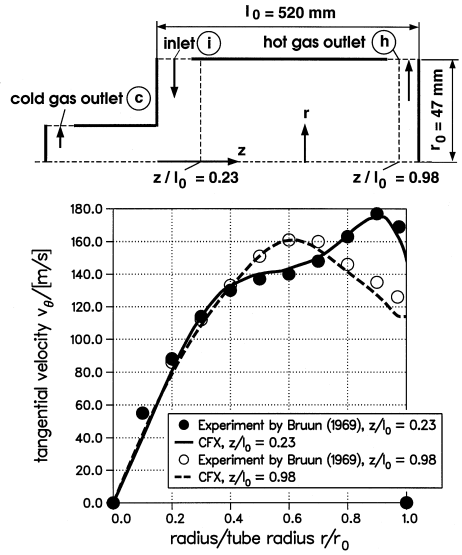

Fig. 8. Comparison code—experiment: tangential velocity profiles by the dimensionless tube length $z/l_0 = 0.23$ ($z = 119.6$ mm) and $z/l_0 = 0.98$ ($z = 509.6$ mm).

$\xi_{r,w} = 0.12$. This fluid increases its tangential velocity (Fig. 8) and develops the beginning of the backflow at the dimensionless radius $r/r_0 = 0.6$ (Fig. 6, tube radius $r_0 = 47$ mm). The backflow increases continuously, due to supply from the radially expanding fluid. Near the wall, 27% of the inlet mass flow expands radially inwards and is mixed together with the part $\xi_{r,w} = 0.12$. Near the left end of the tube, the resulting backflow is divided into an outwards directed part of $\xi_{r,i} = 0.15$, which mixes with the inlet flow and the fraction of the cold gas outlet flow $\xi_c = 0.24$. As a conclusion, an axial-radial circulating secondary flow $\xi_{r,i} = 0.15$ can be indicated, which receives energy from the cold gas, transmitted radially outwards to the hot gas.

The correlation from Keyes (see equation (11)) leads to a Reynolds number $Re_{\theta,p} = 1.4 \cdot 10^6$ and a ratio μ_T/μ_L between turbulent and laminar viscosity of 394. The resulting tangential velocity profiles are shown in Fig. 8. The inlet tangential velocity from 199 m s^{-1} decreases until the dimensionless tube length reaches $z/l_0 = 0.23$ at a maximal velocity of 175 m s^{-1}. The tangential velocity dissipates in the outside area ($r/r_0 > 0.7$) in axial direction. The velocity close to the wall ($r/r_0 = 0.975$) decreases from 162 m s^{-1} ($z/l_0 = 0.23$) to 114 m s^{-1} ($z/l_0 = 0.98$).

The radial pressure gradient:

$$\frac{\partial p}{\partial r} = \rho \frac{v_\theta^2}{r}, \tag{17}$$

causes a radially expanding fluid. The inwards directed transfer of rotational impulse is connected with the change of position of the maximal tangential velocity radially inwards, e.g., to the dimensionless radius $r/r_0 = 0.6$ at the hot gas tube end (dimensionless tube length $z/l_0 = 0.98$). The calculated tangential velocity profiles approximately agree with the measurements.

Table 1
CFX-calculated cold/hot gas total temperature differences to the inlet total temperature for several turbulent Prandtl numbers Pr_T and results measured by Bruun.

	$\Delta T_{t,c}$ (K)	$\Delta T_{t,h}$ (K)
CFX ($Pr_T = 0.9$)	−10.5	3.3
CFX ($Pr_T = 1.8$)	−13.7	4.3
CFX ($Pr_T = 2.7$)	−15.7	5.0
CFX ($Pr_T = 9.0$)	−20.0	6.3
Experiment by Brunn	−20.0	6.0

The total temperature differences of the hot and cold gas in dependence of the turbulent Prandtl number are given in Table 1. The total temperature differences can be enlarged by increasing the turbulent Prandtl number. The mechanical work flux increases related to the diffusive energy flux (see equation (7)). The increase of the turbulent Prandtl number Pr_T from 0.9 to 9.0 (see Table 1) produces the same cold gas total temperature difference $\Delta T_{t,c} = -20$ K as in Bruun's experiment.

The energetic processes in the vortex tube flow can be analyzed by using the numerical CFX results. Temperature changes during the expansion of the cold gas, from the beginning of the backflow C1 in direction of the cold gas outlet C2, are shown in Fig. 9. The cold gas

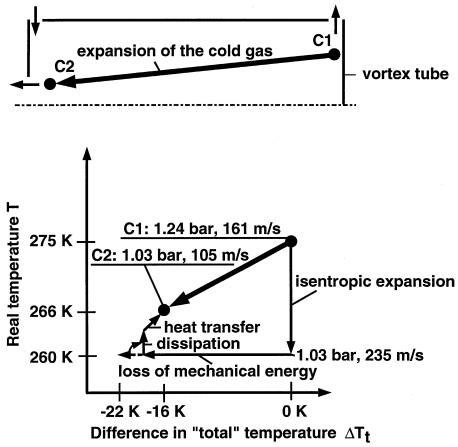

Fig. 9. Changes of real and total temperatures for the expansion of the cold gas (C1: dimensionless radius $r/r_0 = 0.625$, C2: dimensionless radius $r/r_0 = 0.275$) according to the CFX results for $Pr_T = 9$.

expands from 1.24 to 1.03 bar and decreases its velocity from 161 to 105 m s^{-1}. The temperature is reduced from 275 to 266 K, the difference ΔT_t of the total temperature is -16.4 K.

The decrease of the total energy of the cold gas can also be explained by the represented processes in the T–ΔT_t-diagram in Fig. 9. The velocity increases through isentropic expansion from the pressure at state C1 to those at state C2 from 161 to 235 m s^{-1}. The temperature decreases to 260 K. For an additional decrease of the total temperature it is necessary that the cold gas looses kinetic energy too. The difference of the kinetic energy between 235 m s^{-1} (state after isentropic expansion) and 105 m s^{-1} (state C2) equals a total temperature difference of -22 K. This total temperature difference is reduced to $\Delta T_{t,c} = -16$ K by dissipation and heat transfer, causing in turn a temperature rise from 260 to 266 K. The results explain that the expansion results in kinetic energy production, which is transferred to the hot gas and to a lesser portion converted back into heat directly by dissipation.

The state of change for the dissipation of the hot gas is shown in Fig. 10. The pressure is reduced from state H1 (1.45 bar) to H2 (1.38 bar) by the influence of the wall friction. The equivalent isentropic expansion produces an increase of the velocity from 207 to 225 m s^{-1}. The difference of the kinetic energy between 225 m s^{-1} (state after isentropic expansion) and 119 m s^{-1} (state H2) dissipates and causes an 18 K temperature increase (from 269 to 287 K). Additionally, the hot gas receives mechanical energy from the inner layers, which dissipates as well and leads to a further temperature increase, which is however partly compensated by heat transfer to the cold gas. As a consequence, the additional net temperature increase amounts to 6 K, leading to 293 K in state H2.

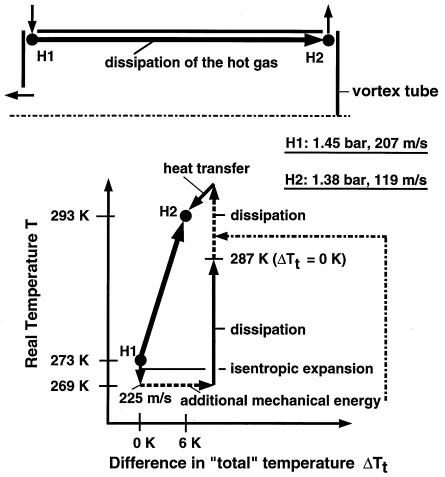

Fig. 10. Changes of real and total temperatures for the dissipation of the hot gas (dimensionless radius $r/r_0 = 0.875$) according to the CFX results for $Pr_T = 9$.

5. Conclusions

The energy transfer from the cold to the warm gas has been explained by mechanical work transfer. In the vortex tube the fluid layers rotate with different angular velocities. Due to friction, inner gas layers are decelerated by layers near the tube wall, causing transfer of mechanical energy from the cold to the hot gas. The numerical results show that it is possible to calculate the compressible flow and energy separation phenomena numerically. In order to assess the energy transfer, terms of work done on fluid by viscous forces (shear stress-induced-mechanical work) has to be integrated into the numerical model.

For the numerical model the usage of an axisymmetric model with radially assigned inlet and outlets is possible. With the pressure drop from the hot to the cold gas outlet the cold gas flow fraction ξ_c could be adjusted. The application of the k–ε-model leads to substantial differences between measured and calculated tangential velocity profiles. For the calculation of the turbulent viscosity, the k–ε-model can be replaced by the correlation from Keyes [13]. The transient solution procedure of the CFX flow model needed two iteration processes, because the direct specification of pressure values at both outlets leads to numerical instabilities. The strength of the energy separation can be fitted to both measured total temperature differences (cold/hot gas to the inlet total temperature) by increasing the turbulent Prandtl number, leading to a damping of the turbulent diffusion in favour of the transfer of mechanical work. Furthermore, by means of an axial-radial flow diagram, a circulating secondary flow—receiving energy from the cold gas, transmitted outward to the hot gas–could be identified. A comparison of the change of state for cold and hot gas shows that in the cold gas the expansion and in the hot gas the dissipation predominates. The expansion causes a cooldown effect in the cold gas. Mechanical work is transferred from the cold to the hot gas by friction, intensifying dissipation processes there, which result in a temperature increase of the hot gas portion.

Acknowledgements

The authors thank the 'Institut Thermo-Fluiddynamik (J. U. Keller) of the University Siegen (Germany)' and the 'Department of Physics (B. Ahlborn) of the University of British Columbia, Vancouver (Canada)' for fine support and many fruitful discussions and incentives. The research project was partly sponsored by the 'Wilhelm und Günther Esser Stiftung'.

References

[1] G.H. Ranque, Expériences sur la détente giratoire avec production simultanées d'un échappement d'air chaud et d'air froid, Journal de Physique et le Radium IV(1933) 112–114.

[2] R. Hilsch, Die Expansion von Gasen im Zentrifugalfeld als Kälteprozeß, Z. Naturforschung 1 (1946) 208–214.

[3] J. Camiré, Experimental investigation of vortex tube concepts, Department of Physics (Prof. Dr B. Ahlborn), University of British Columbia, Vancouver, Canada, 1995.

[4] K. Stephan, S. Lin, M. Durst, F. Huang, D. Seher, Investigation of energy separation in a vortex tube, International Journal Heat Mass Transfer 26 (3) (1983) 341–348.

[5] A. Rogowski, E. Schütt, R. Heinisch, Arbeit in der technischen Thermodynamik, Forschung im Ingenieurwesen 59 (11/12) (1993) 229–233.

[6] R. Heinisch, A. Rogowski, E. Schütt, Die Energiewandlung bei der Strömung von Fluiden, Brennstoff-Wärme-Kraft (BWK) 48 (6) (1996) 59–63.

[7] W. Fröhlingsdorf, Unterschungen zur kompressiblen Strömung und Energietrennung im Wirbelrohr nach Ranque und Hilsch, Dissertation, Ruhr-Universität-Bochum, 1997 (Shaker Verlag Aachen, Berichte aus der Strömungstechnik, ISBN: 3–8265–2829–8).

[8] FLOW3D, Release 3.2: User Manual, AEA Industrial Technology, U.K. 1992.

[9] R.B. Bird, W.E. Stewart, E.N. Lightfoot, Transport Phenomena, Wiley, New York, 1960.

[10] C.D. Fulton, Ranque's Tube, Journal of the ASRE 58 (1950) 473–478.

[11] M. Kurosaka, Acoustic streaming in swirling flow and the ranque-hilsch (vortex-tube) effect, Journal Fluid Mechanics 124 (1982) 139–172.

[12] H.H. Bruun, Experimental investigation of the energy separation in vortex tubes, J. Mechanical Engineering Science 11 (6) (1969) 567–582.

[13] J.J. Keyes, Jr., An Experimental study of gas dynamics in high velocity vortex flow, in: Proceedings of the Heat Transfer and Fluid Mechanics Institute, Stanford University, Oak Ridge National Laboraty, Tennessee, 1960, pp. 31–46.